

# Optical model-solution to the competition between a pseudogap phase and a Mott-gap phase in high-temperature cuprate superconductors

Tanmoy Das, R. S. Markiewicz, and A. Bansil

*Physics Department, Northeastern University, Boston MA 02115, USA*

(Dated: April 29, 2021)

We present a theoretical framework for a quantitative understanding of the full doping dependence of the optical spectra of the cuprates. In accord with experimental observations, the computed spectra show how the high-energy Mott features continue to persist in the overdoped regime even after the mid-infrared (MIR) peak originating from the pseudogap has collapsed in a quantum critical point. In this way, we reconcile the opposing tendencies of the MIR and Mott peaks to shift in opposite directions in the optical spectra with increasing doping. The competition between the pseudogap and the Mott gap also results in rapid loss of spectral weight in the high energy region with doping.

PACS numbers: 74.20.-z, 74.20.Mn, 74.25.Gz, 74.25.Jb

## I. INTRODUCTION

Most experiments on the cuprates show that when the Mott insulating state is doped with electrons or holes the gap feature in the spectrum moves to lower energies and collapses at a quantum critical point, consistent with the notion that electron correlation effects in the Mott state weaken systematically with doping.<sup>1-3</sup> In sharp contrast, optical experiments reveal a substantially more complex picture in that the doping of the Mott insulator induces a new mid-infrared (MIR) feature<sup>4-7</sup>, which collapses with doping much as seen in other experiments, but at the same time a high-energy Mott feature persists even into the overdoped system with its spectral weight shifting to the MIR feature with increasing doping.<sup>8-13</sup> In fact, the Mott feature not only persists in the optical experiments, but it moves to *higher* energies with doping, suggesting that strong electron correlation effects continue to play an important role in the cuprates at all dopings. Modelling and understanding the optical spectra of the cuprates thus becomes of key importance in unravelling the routes by which the Mott insulator turns itself into a superconductor, a transition that remains poorly understood.

The question of correlations has been traditionally framed in terms of a Slater picture of itinerant electrons where an insulator forms a gap via the development of a long range magnetic order, or a Mott picture in which the metal-insulator transition is driven by a local condition of no double occupancy. Although the Slater or the Mott picture is often invoked, many materials lie in the crossover regime where the electronic states are not well described as being either fully itinerant or fully localized. Such materials are often endowed with unique and exotic properties and are of great current interest from the viewpoint of fundamental physics as well as potential for applications. The strength of electron correlations in the cuprates has been a matter of considerable debate since the discovery of these fascinating materials.<sup>14</sup>

We have obtained the optical spectra within the framework of a one band Hubbard model where the self-energy

is obtained self-consistently in an intermediate coupling scenario to account for spin and charge fluctuations via a computation of the susceptibility over the entire doping range. We emphasize that the present model essentially does not involve any free parametrization in that the bare LDA dispersion is taken to be the CuO<sub>2</sub> band (in the tight-binding form) and a doping-independent bare  $U$  is chosen to reproduce the experimental charge-transfer gap at half-filling. The screened  $U$  at various doping levels is then computed due to charge fluctuations<sup>15,16</sup>, which self-consistently induce a low-energy magnetic order in the in-gap states resulting in a pseudogap in the underdoped system. Our computations reproduce quantitatively the experimentally observed doping evolution of not only the shifts in the positions of the MIR and Mott features, but also the rapid transfer of spectral weight from the high to the low energy region with increasing doping. The theoretical shifts of the MIR feature with doping are in accord with angle-resolved photoemission spectroscopy (ARPES)<sup>17</sup> and other spectroscopic probes. We emphasize that existing approaches invoking either strong or weak coupling scenarios fail to capture the essence of the doping evolution of the optical spectra.

## II. OPTICAL SPECTRA IN ELECTRON AND HOLE DOPED CUPRATES

Fig. 1 shows one of our key results. The computed evolution of the optical conductivity  $\sigma(\omega)$  is seen to be in excellent accord with measurements on electron-doped Nd<sub>2-x</sub>Ce<sub>x</sub>CuO<sub>4</sub> (NCCO) and hole doped La<sub>2-x</sub>Sr<sub>x</sub>CuO<sub>4</sub> (LSCO)<sup>11,13</sup>. All the spectra show a nearly isosbetic or equal absorption point near 1.3 eV (1 eV for LSCO) [black vertical line], consistent with the experimental behavior<sup>18</sup>. The doping evolution is completely different on opposite sides of this isosbetic point. Above this point, the spectrum is dominated by a broad hump feature associated with the Mott gap. At half-filling, only this feature is present and the calculated optical spectra show an insulating gap whose energy, structure, and

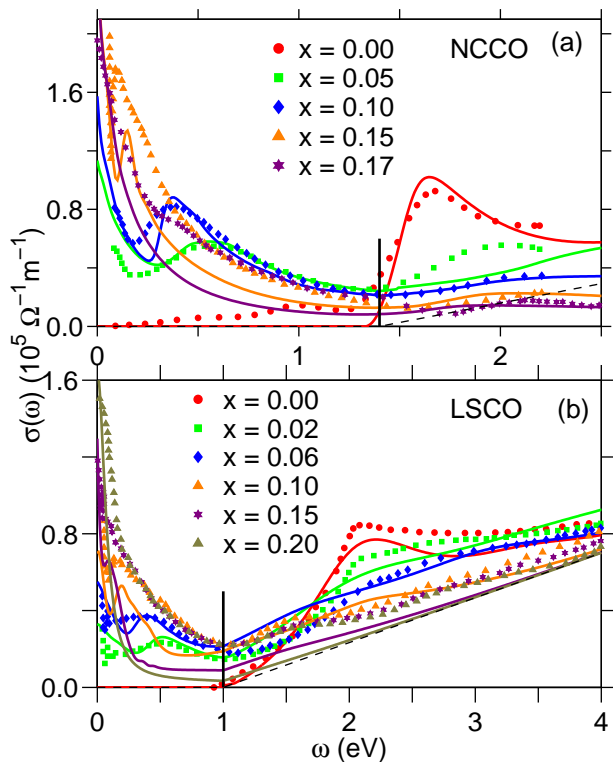


FIG. 1: (color online) Comparison between calculated optical spectra and experiments in NCCO in (a) and LSCO in (b). Experimental results for NCCO are taken from Ref. 13, except for  $x = 0.17$ , which including LSCO data, are from Ref. 11. The  $x = 0.17$  dataset for NCCO includes a background subtraction to match the former dataset<sup>20</sup>. Dashed line gives the background contribution added to the theoretical spectrum at  $x = 0$  [Ref. 14].

intensity match remarkably with measurements<sup>11,13</sup>. As doping increases, the high energy peak shifts to higher energy and broadens and its spectral weight is transferred to the Drude and MIR peaks. The MIR peak shifts to lower energy with doping and gradually sharpens. Note that in both samples at the highest doping, when the MIR peak collapses into the Drude peak, Mott-gap features still persist in the spectrum. The doping evolution also shows similar behavior in other cuprates<sup>8-13,19</sup>. Notably, our calculations also describe the anomalous  $\sigma \sim 1/\omega$ -dependence found in most cuprates associated with magnetic scattering.

### A. Origin of optical dichotomy

Fig. 2 helps delineate the microscopic origin of these features by comparing the spectral intensities relevant for ARPES and optical spectra at a representative doping of  $x = 0.10$  for NCCO; similar analysis for LSCO is not shown for brevity. In the computed ARPES spectrum in Fig. 2(a), the underlying LDA dispersion is clearly visible, but the spectral weight has split into four subbands,

as is also the case in variational cluster calculations<sup>21</sup>. The highest and lowest bands are an incoherent residue of the undressed bands, which we will refer to as upper and lower Hubbard bands. The two inner bands are coherent in-gap states split by a spin density wave induced AFM gap into upper and lower magnetic bands. The in-gap states and the high energy Hubbard bands are separated by high-energy kinks (‘waterfalls’) predominantly associated with magnetic excitations, as observed universally in all cuprates by ARPES<sup>22-24</sup>, and found in quantum monte carlo (QMC)<sup>25</sup> and variational<sup>21</sup> calculations.

The corresponding optical spectrum in Fig. 2(b) consists of three main regions marked by shading of different color: (1) The low frequency Drude region for  $\omega \lesssim 30\text{meV}$ ; (2) The MIR region; and, (3) the high energy Mott gap region for  $\omega \gtrsim 1.5\text{eV}$ . We concentrate here on the MIR and Mott-gap regions, and return below to comment on the Drude region. The interband optical absorption is proportional to the joint density of states (JDOS), so that at each energy we can construct a ‘source map’ showing the filled states which make a strong contribution to the transition, and a ‘sink map’ showing the contribution of the corresponding empty states. Figs. 2(d) and (e) show the states responsible for the optical transitions along the high symmetry lines at representative photon energies of  $\omega = 0.5\text{eV}$  near MIR peak and  $\omega = 2\text{eV}$  around the high energy peak (vertical bars in Fig. 2(b)). At  $\omega = 0.5\text{eV}$ , the transitions are confined within the in-gap states only, whereas at  $\omega = 2\text{eV}$ , the optical subbands involve predominantly the incoherent region. The depletion in the optical spectral weight near the isosbetic point in Fig. 1 and in Fig. 2(b) is thus associated with the ‘waterfall’ region marked by arrows in the ARPES spectrum in Fig. 2(a)<sup>18</sup>.

The total optical spectral weight obtained in Fig. 2(b) is the integral of the JDOS times the band velocity. The role of the latter factor is explicated in Fig. 2(c), where contributions to  $\sigma$  are plotted as a function of photon energy  $\omega$  and momentum  $k$ . Although the source-sink map shows a symmetry about the  $(\pi, 0)$  point, the quasiparticle velocity is low along the  $\Gamma \rightarrow (\pi, 0)$  direction [cyan solid line in Fig. 2(c)], leading to greatly reduced spectral intensity associated with those regions. In contrast, the large quasiparticle velocity in the other two directions is responsible for two distinctive intense streaks (labelled d and e). The MIR peak is clearly dominated by the antinodal quasiparticles, whereas the high energy hump stems from a wider  $k$ -range.

### B. Competition between Pseudogap and Mott gap

Fig. 3 summarizes our results and elaborates upon the competition between the collapse of the pseudogap in the coherent bands at a critical doping, and the persistence of the Mott gap in the incoherent bands. The gaps extracted from the optical spectra are now compared with other experimental data for various electron-

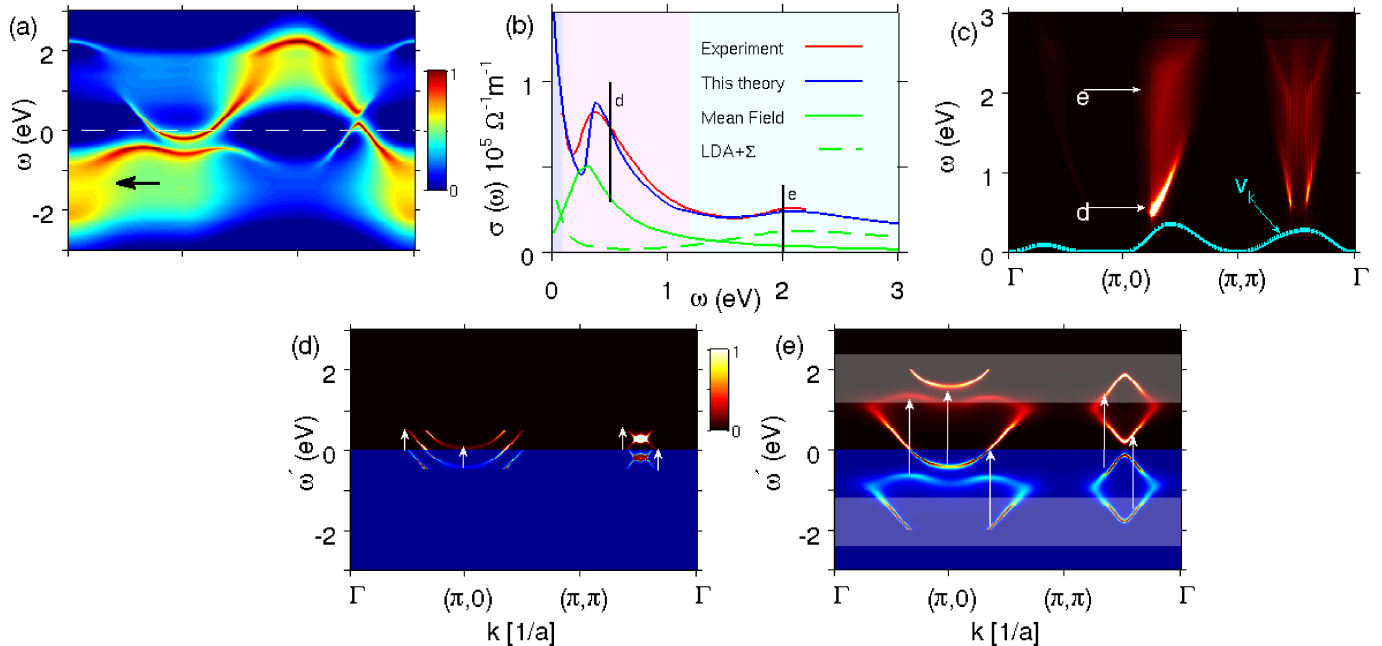


FIG. 2: (Color online) Connection between optical spectra and spectral intensity maps in NCCO. (a) Computed spectral intensity (on log scale) as a function of  $\omega$  along the high symmetry lines at a representative doping of  $x = 0.10$ . (b) Calculated optical spectra are compared with the corresponding experimental results<sup>13</sup>. Green solid line gives the spectrum calculated with coherent bands only, i.e. without the self-energy. Dashed green line is based on using LDA bands with self-energy correction but without the pseudogap. The shaded regions of different colors (left to right) approximately mark Drude, MIR and high energy regions. Two vertical black lines indicate the photon energies at which frames (d) and (e) are calculated. (d), (e) give source and sink maps corresponding to the optical transitions at fixed photon energy  $\omega$  along the high symmetry directions. White vertical arrows indicate the photon energy connecting source and sink points in a particular transition. White shaded region in (e) highlights the incoherent part of the spectral weight, not visible in (d). (c) Optical spectrum as a function of photon energy is plotted along the high symmetry lines. Cyan line gives the band velocity as a function of  $k$  (arbitrary units). The two white arrows indicate the two photon energies at which (d) and (e) are calculated.

and hole-doped cuprates. The pseudogap seen in the optical spectrum corresponds to the true AFM gap, and its doping evolution is in good agreement with optical, ARPES<sup>2,26,31</sup> and resonant inelastic x-ray scattering (RIXS)<sup>27</sup> results. Both ARPES and MIR data predict a QCP near  $x = 0.17$ <sup>32,33</sup> consistent with the present theoretical predictions. In contrast, the Mott gap shows the opposite doping dependence to the pseudogap, increasing slowly with doping. Although the Mott gap does not show a real QCP, it rapidly loses intensity with doping.

Similar results are found in hole doped LSCO<sup>11</sup>, and other layered cuprates, including Bi<sub>2</sub>Sr<sub>2</sub>CaCu<sub>2</sub>O<sub>8+ $\delta$</sub>  (Bi2212)<sup>9</sup>, YBa<sub>2</sub>Cu<sub>3</sub>O<sub>6+x</sub> (YBCO)<sup>8</sup>, Tl<sub>2</sub>Ba<sub>2</sub>CuO<sub>6+ $\delta$</sub>  (TBCO), and HgBa<sub>2</sub>Ca<sub>2</sub>Cu<sub>3</sub>O<sub>8+ $\delta$</sub>  (HBCO)<sup>19</sup> as well as in x-ray absorption spectroscopy<sup>20</sup> and QMC computations.<sup>34</sup> Figure 3 also includes data on the MIR gap for LSCO, Bi2212 and YBCO and the pseudogap obtained from a wide range of experimental data, including a recent detailed survey<sup>28</sup> (see Fig. 3 caption). In the intermediate and high doping regimes, there is very good agreement between the MIR and other measures of the

pseudogap, while the MIR data provides important evidence for the rapid growth of the pseudogap in the deeply underdoped regime, consistent with theory. We note that while all the hole-doped cuprates seem to have a very similar doping dependence of the pseudogap, there are subtle differences with electron doped cuprates, including the steepness of the rise at low doping and the exact position of the QCP.<sup>28,35</sup> The former difference seems to be correlated with the doping dependence of the screened Hubbard  $U$ 's, also shown in Fig. 3. Since the doping dependence is mainly a screening effect,<sup>15,16</sup> the difference is probably due to the strong screening associated with the van-Hove singularity (VHS) on the hole-doped side.

While a strong case can be made that in electron-doped cuprates the pseudogap is associated with a coexisting  $(\pi, \pi)$  AFM order, the nature of the pseudogap in hole doped cuprates is not well understood. There is growing consensus that it originates from some form of density-wave like competing order (which could include coupling to phonons)<sup>36-38</sup>, and may actually also involve several competing modes, again due to proximity to the

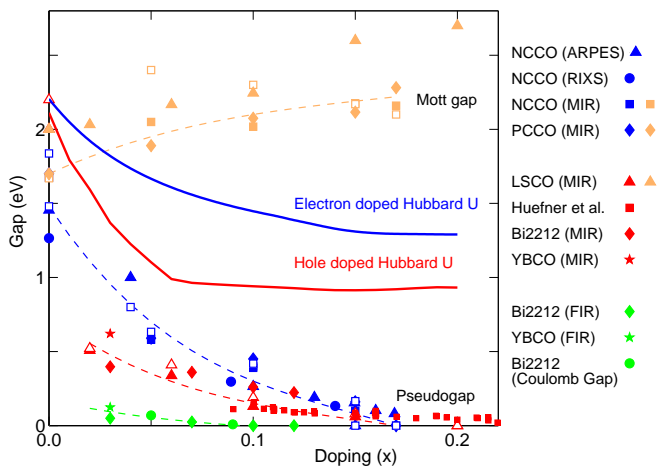


FIG. 3: (Color online) Contrasting doping dependences of the MIR and Mott gaps in the cuprates. Present theoretical results are compared to optical data<sup>10,11,13</sup> and pseudogap data measured by ARPES<sup>2,26</sup> and RIXS<sup>27</sup> for electron doped NCCO and many other probes for hole doped cuprates. The red squares are the pseudogap for four different layered compounds [Bi2212, YBCO, TBCO and HBCO] as they are obtained from ARPES, tunneling, Raman, Andreev reflection, and heat capacity experimental data (reproduced from a detailed survey, Ref. 28). The red diamond and star symbols represent independent MIR and green diamond and star give FIR gaps measured simultaneously in optical spectra of Bi2212 and YBCO<sup>29</sup>, while the green circles represent a Coulomb gap seen in ARPES<sup>30</sup> [energy values are obtained assuming a ratio  $2\Delta/k_B T = 4$ ]. In all cases, open symbols of same colors are the corresponding theory which are obtained self-consistently at each doping. Shown also are the computed screened value of  $U$  (solid lines)<sup>15,16</sup> used in these calculations. The dashed lines are guides to the eye for the Mott gap (gold), the pseudogaps for electron (blue) and hole (red) doping, and the FIR and Coulomb gaps (green).

VHS<sup>39</sup>. However, in our earlier study in Ref. 33, which compared several possible competing order phases, we demonstrated that the shape and doping dependence of the pseudogap is remarkably insensitive to the particular order so long as the competing order vanishes in a QCP near optimal doping.

While our present calculations reproduce the gap structures of cuprates, particularly on energy scales  $\geq 100$  meV, additional effects can arise at lower energies, including coupling to phonons and impurities. In particular, Lupi *et al.*<sup>29</sup> find in several cuprates that in addition to the MIR feature there is an additional far-infrared (FIR) peak which appears near 10% doping and shifts to higher energies at lower doping (green diamond and star symbols in Fig. 3). This seems to be a disorder effect, and has a similar doping dependence to the so-called Coulomb gap seen in ARPES (green circles) in the low-temperature region of Bi2212.<sup>30</sup>

We emphasize that the dichotomy between the pseudogap and Mott gap and the presence of the QCP are robust features of cuprates as the computations do not

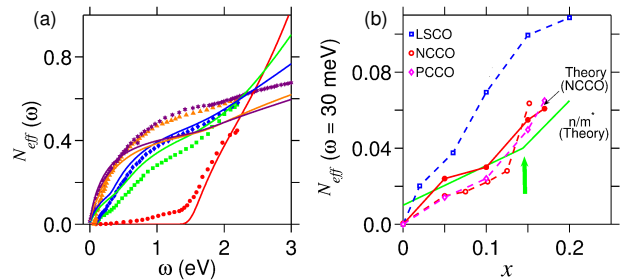


FIG. 4: (Color online) Optical sum rule and spectral weight transfer. (a) Effective number of electrons  $N_{eff}(\omega)$  calculated from the optical spectra in Fig. 1 is compared with experimental data<sup>12,13</sup> on NCCO. Results for LSCO are similar and are not shown for brevity. (b) Low energy weight  $N_{eff}$  at  $\omega = 30$  meV as an estimate of Drude weight, compared with experimental results on various cuprates<sup>10–12</sup>. Green line gives the direct computation of the normalized Drude weight  $n/m^*$ .

involve any free parametrization except the bare doping-independent value of  $U = 1.7$  eV at half-filling. We have computed the doping dependence of  $U$  due to the screening effects of charge fluctuations<sup>15,16</sup> and obtained effective  $U$  values are shown Fig. 3.

### III. OPTICAL SUM RULE

Finally, we use the integrated optical spectral weight to illustrate the Mott gap collapse. The effective electron number (per Cu atom),  $N_{eff}(\omega)$ , can be defined in terms of the optical conductivity integrated up to an energy  $\omega$ :

$$N_{eff}(\omega) = \frac{2m_0V}{\pi e^2 \hbar N} \int_0^\omega \sigma(\omega') d\omega', \quad (1)$$

where  $m_0$  and  $e$  are the free electron mass and charge, respectively, and  $N$  is the number of Cu-atoms in a cell of volume  $V$ . The results in Fig. 4(a) show how rapidly spectral weight shifts to low energies with doping, correctly reproducing the experimental behavior as well as dynamical mean-field calculations<sup>14</sup>, but incompatible with strong coupling models (such as the  $t-J$  or  $U \rightarrow \infty$  Hubbard model) where one assumes no double occupancy of Cu sites. The present intermediate coupling model of Mott gap collapse on the other hand properly captures these spectral weight transfers as a function of doping.

Our model also predicts the Drude weight  $\propto \sum_{\mathbf{k}} n_{\mathbf{k}}/m_{\mathbf{k}}^*$ , which can be compared to an experimental estimate, taken as  $N_{eff}$  at a characteristic energy  $\omega = 30$  meV in Fig. 4(b) for NCCO<sup>12</sup>, and with results for  $\text{Pr}_{2-x}\text{Ce}_x\text{CuO}_4$  (PCCO)<sup>10</sup> and LSCO<sup>11</sup>. Even here the agreement is quite good. Interestingly, at low doping the Drude weight increases almost linearly with  $x$ . Within our model, this simply reflects scaling with the area of the FS pockets in the pseudogap state. At optimal doping, the weight shows a sharp jump (green arrow) associated with the appearance of the hole pocket. This topological FS transition is an intrinsic feature of

the model and has been found in NCCO near  $x \approx 0.15$  by several experimental probes such as ARPES<sup>2</sup>, Hall effect<sup>40</sup>, and superconducting penetration depth<sup>32</sup>. For LSCO (blue symbols), experiments<sup>11</sup> show a similar linear behavior of the Drude weight, which also corresponds to the doping dependence of the area of the FS pocket<sup>41</sup>. The peak around  $x \sim 0.2$  corresponds to the doping of the Van Hove singularity.

#### IV. INTERMEDIATE COUPLING MODEL

We evaluate the self-energy  $\Sigma$  as a convolution over the green function  $G$  and the interaction  $W \sim U^2\chi$  (including the full spectrum of charge and spin fluctuations within the random phase approximation (RPA)) as<sup>17,42,43</sup>,

$$\Sigma(\mathbf{k}, \sigma, i\omega_n) = \frac{1}{2}U^2Z \sum_{\mathbf{q}, \sigma'}^l \eta_{\sigma, \sigma'} \int_0^\infty \frac{d\omega_p}{2\pi} G(\mathbf{k} + \mathbf{q}, \sigma', i\omega_n + \omega_p) \Gamma(\mathbf{k}, \mathbf{q}, i\omega_n, \omega_p) \text{Im}[\chi_{\text{RPA}}^{\sigma\sigma'}(\mathbf{q}, \omega_p)]. \quad (2)$$

where  $\sigma$  is the spin index and the prime over the  $\vec{q}$  summation means that the summation is restricted to the magnetic Brillouin zone. Here the spin degree of freedom  $\eta_{\sigma, \sigma'}$  takes the value of 2 for the transverse direction and 1 for both longitudinal and charge modes. In the underdoped region, the pseudogap is modelled by an antiferromagnetic (AFM) order parameter, resulting in  $G$ ,  $\chi$  and  $\Sigma$  becoming  $2 \times 2$  tensors<sup>44</sup>. We define a total self-energy as  $\Sigma^t = US\tilde{\tau}_1 + \Sigma$ , where  $\tilde{\tau}_1$  is the Pauli matrix along the  $x$ -direction and  $US$  is the AFM gap defined below. The self-energy  $\Sigma^t$  contains essentially two energy scales: (i) it gives rise to the SDW with an additional renormalization of the overall quasiparticle dispersions in the low energy region, and (ii) at higher energies it produces the Hubbard bands. We use a modified self-consistent scheme, referred to as quasiparticle- $GW$  (QP- $GW$ )-scheme in which  $G$  and  $W$  are calculated from an approximate self-energy  $\Sigma_0^t(\omega) = US\tilde{\tau}_1 + (1 - Z^{-1})\omega\tilde{\mathbf{1}}$ , where the renormalization factor  $Z$  is adjusted self-consistently to match the self-energy  $\Sigma^t$  at low energy.<sup>16,24,43</sup> The vertex correction  $\Gamma(\mathbf{k}, \mathbf{q}, \omega, \omega_p)$  in Eq. 2 is taken as its first order approximation (Ward's identity) as  $\Gamma(\mathbf{k}, \mathbf{q}, \omega, \omega_p) = 1/Z$ . Since the  $k$ -dependence of  $\Sigma$  is weak<sup>24</sup>, we further simplify the calculation by assuming a  $k$ -independent  $\Sigma$ , which we calculate at a representative point  $k = (\pi/2, \pi/2)$ .

Our model is nearly parameter free. We take the dispersions directly from the LDA calculations, accurately fitted by a one band tight-binding model<sup>45</sup>, without any adjustment of the resulting parameters. The susceptibilities are calculated numerically, with no further approximations, while the renormalization constant  $Z$  is determined self-consistently. We have performed realistic Kanamori screening calculations due to charge fluctuations to obtain a self-consistent value of  $U$  and order

parameter  $\phi$  at each doping starting from a doping independent bare  $U = 1.7$  eV which reproduces the charge transfer gap at half-filling.<sup>15,16</sup>

The optical conductivity,  $\sigma(\omega)$ , is calculated using the standard linear response theory using the above  $\Sigma$ -dressed single particle states. At high energies, we subtract off a linear-in- $\omega$  background from the experimental spectra associated with interband transitions to higher-lying bands not included in the present one-band calculations, consistent with supplementary Fig. 4 of Ref. 14. While keeping fixed the calculated weights of the Drude peaks, we have phenomenologically broadened the spectra with additional constant impurity scattering rates, similar to the universal form found in experiments on NCCO<sup>13</sup>, LSCO<sup>11</sup>, and Bi2212<sup>9</sup>.

#### V. DISCUSSION AND CONCLUSION

While the  $(\pi, \pi)$  AFM order is known to be a robust feature in electron doped cuprates, in the hole doped case the exact nature of the pseudogap is unknown, and is likely to be incommensurate and possibly associated with charge order. This is consistent with our earlier study of ARPES<sup>33</sup>, where we compared several possible competing ordered phases and demonstrated that the shape and doping dependence of the pseudogap is remarkably insensitive to the particular order so long as the competing order vanishes in a quantum critical point near optimal doping. This conclusion should hold even more strongly for the optical spectrum. Note that we have included all the charge and spin fluctuations in our calculations – the particular leading instability will only lead to a small rearrangement of spectral weight in the low energy regime, leaving most of the optical spectrum virtually unchanged.

We note that recent Gutzwiller approximation (GA) + RPA calculations find a number of nesting instabilities in hole-doped cuprates, resulting in a number of competing, incommensurate density-wave orders.<sup>39</sup> Since the instabilities depend on the bare susceptibilities, they are located at virtually the same  $q$ -values in both the spin and charge (electron-phonon) channels. Thus, the resulting optical spectra should be very similar in both cases.

Finally, we note that the same model can be used to explore the role of magnetic fluctuations as the pairing bosons for superconductivity.<sup>46</sup> While the study of Ref. 46 revealed a significant contribution from magnetic fluctuations, it was found that fluctuations in different frequency ranges could act cooperatively to greatly enhance  $T_c$ . This suggests that phonons could play a similar cooperative role which could explain the isotope effect.<sup>36</sup>

In summary, we have shown that our model framework explains the salient features of the optical spectra of cuprates and their evolution with doping at a quantitative level. The rapid loss of high energy spectral weight and the associated shift of the MIR peak to low energies in the optical spectra with increasing doping reflects collapse of the pseudogap order [here taken

as a  $(\pi, \pi)$  AFM], and the presence of a QCP near optimal doping in the coherent in-gap states. By contrast, the Mott gap in the incoherent states persists at all dopings including, in particular, the overdoped regime. The aforementioned coherent and incoherent states are connected via a high-energy kink driven predominately by magnetic excitations. In the magnetic excitation spectrum, the dominant excitations lie in the waterfall region, while the remnant of the low-energy magnetic resonance mode<sup>36</sup> is less significant<sup>24</sup>. Our model self-energy scheme would provide a tangible basis for modelling other spectroscopies (e.g., angle-resolved photoemission<sup>17,43</sup>, scanning-tunnelling<sup>33</sup>, inelastic light scattering<sup>27</sup>, positron-annihilation<sup>47</sup>) of the cuprates and

other materials.

### Acknowledgments

This work was supported by the US Department of Energy, Basic Energy Sciences contract DE-FG02-07ER46352, and benefited from the allocation of supercomputer time at NERSC and Northeastern University's Advanced Scientific Computation Center (ASCC). RSM's work has been partially funded by the Marie Curie Grant PIF-GA-2008-220790 SOQCS.

- 
- <sup>1</sup> A. Damascelli, Zahid Hussain, and Zhi-Xun Shen, *Rev. Mod. Phys.* **75**, 473 (2003).
- <sup>2</sup> N.P. Armitage, F. Ronning, D. H. Lu, C. Kim, A. Damascelli, K. M. Shen, D. L. Feng, H. Eisaki, Z.-X. Shen, P. K. Mang, N. Kaneko, M. Greven, Y. Onose, Y. Taguchi, and Y. Tokura, *Phys. Rev. Lett.* **88**, 257001 (2002).
- <sup>3</sup> M. Le Tacon, A. Sacuto, A. Georges, G. Kotliar, Y. Gallais, D. Colson, and A. Forget, *Nature Physics* **2**, 537 (2006).
- <sup>4</sup> K. Haule, and G. Kotliar, *Europhys. Lett.* **77**, 27007 (2007).
- <sup>5</sup> S. Chakraborty, Dimitrios Galanakis, and Philip Phillips, *Phys. Rev. B* **78**, 212504 (2008).
- <sup>6</sup> Mishchenko, N. Nagaosa, Z.-X. Shen, G. De Filippis, V. Cataudella, T. P. Devereaux, C. Bernhard, K. W. Kim, and J. Zaanen, *Phys. Rev. Lett.* **100**, 166401 (2008).
- <sup>7</sup> L. Vidmar, J. Bonca, and S. Maekawa, *Phys. Rev. B* **79**, 125120 (2009).
- <sup>8</sup> S. L. Cooper D. Reznik, A. Kotz, M. A. Karlow, R. Liu, M. V. Klein, W. C. Lee, J. Giapintzakis, D. M. Ginsberg, B. W. Veal and A. P. Paulikas, *Phys. Rev. B* **47**, 8233 (1993).
- <sup>9</sup> J. Hwang, T. Timusk, and G D Gu, *J. Phys.: Condens. Matter*, **19**, 125208 (2007).
- <sup>10</sup> T. Arima, Y. Tokura, and S. Uchida, *Phys. Rev. B* **48**, 6597 (1993).
- <sup>11</sup> S. Uchida, T. Ido, H. Takagi, T. Arima, Y. Tokura, and S. Tajima, *Phys. Rev. B* **43**, 7942 (1991).
- <sup>12</sup> Y. Onose, Y. Taguchi, K. Ishizaka, and Y. Tokura, *Phys. Rev. Lett.* **87**, 217001 (2001).
- <sup>13</sup> Y. Onose, Y. Taguchi, K. Ishizaka, and Y. Tokura, *Phys. Rev. B* **69**, 024504 (2004).
- <sup>14</sup> A. Comanac, Luca de Medici, Massimo Capone, and A. J. Millis, *Nature Physics* **4**, 287 (2008).
- <sup>15</sup> J. Kanamori, *Prog. Theor. Phys.* **30**, 275 (1963).
- <sup>16</sup> R.S. Markiewicz, and A. Bansil, *Phys. Rev. B* **75**, 020508 (2007).
- <sup>17</sup> Susmita Basak, Tanmoy Das, Hsin Lin, J. Nieminen, M. Lindroos, R. S. Markiewicz, and A. Bansil, *Phys. Rev. B* **80**, 214520 (2009).
- <sup>18</sup> Interestingly, the isosbetic point in the optical spectra associated with the 'waterfall' features in ARPES occurs at lower energy in LSCO than NCCO, as does the high energy kink in ARPES spectra<sup>23</sup>.
- <sup>19</sup> McGuire, M. Windt, T. Startseva, T. Timusk, D. Colson, and V. Viallet-Guillen, *Phys. Rev. B* **62**, 8711 (2000).
- <sup>20</sup> C.T. Chen, F. Sette, Y. Ma, M. S. Hybertsen, E. B. Stechel, W. M. C. Foulkes, M. Schuller, S-W. Cheong, A. S. Cooper, L. W. Rupp, Jr., B. Batlogg, Y. L. Soo, Z. H. Ming, A. Krol, and Y. H. Kao, *Phys. Rev. Lett.* **66**, 104 (1991).
- <sup>21</sup> C. Gröber, R. Eder, and W. Hanke, *Phys. Rev. B* **62**, 4336 (2000).
- <sup>22</sup> J. Graf, G.-H. Gweon, K. McElroy, S. Y. Zhou, C. Jozwiak, E. Rotenberg, A. Bill, T. Sasagawa, H. Eisaki, S. Uchida, H. Takagi, D.-H. Lee, and A. Lanzara, *Phys. Rev. Lett.* **98**, 067004 (2007).
- <sup>23</sup> B. Moritz, F. Schmitt, W. Meevasana, S. Johnston, E. M. Motoyama, M. Greven, D. H. Lu, C. Kim, R. T. Scalettar, Z.-X. Shen, T. P. Devereaux, *New Journal of Physics* **11**, 093020 (2009).
- <sup>24</sup> R.S. Markiewicz, S. Sahrakorpi, and A. Bansil, *Phys. Rev. B* **76**, 174514 (2007).
- <sup>25</sup> A. Macridin, M. Jarrell, Thomas Maier, and D. J. Scalapino, *Phys. Rev. Lett.* **99**, 237001 (2007).
- <sup>26</sup> H. Matsui, T. Takahashi, T. Sato, K. Terashima, H. Ding, T. Uefuji, and K. Yamada, *Phys. Rev. B* **75**, 224514 (2007).
- <sup>27</sup> Y. W. Li, D. Qian, L. Wray, D. Hsieh, Y. Xia, Y. Kaga, T. Sasagawa, H. Takagi, R. S. Markiewicz, A. Bansil, H. Eisaki, S. Uchida, and M. Z. Hasan, *Phys. Rev. B* **78**, 073104 (2008).
- <sup>28</sup> S. Hüfner, M.A. Hossain, A. Damascelli, and G.A. Sawatzky, *Rep. Prog. Phys.* **71**, 062501 (2008).
- <sup>29</sup> S. Lupi, D. Nicoletti, O. Limaj, L. Baldassarre, M. Ortolani, P. Calvani, S. Ono, and Yoichi Ando, Preprint at arXiv:0905.0568.
- <sup>30</sup> Z. -H. Pan, P. Richard, Y. -M. Xu, M. Neupane, P. Bishay, A. V. Fedorov, H. -Q. Luo, L. Fang, H. -H. Wen, Z. Wang, and H. Ding, *Phys. Rev. B* **79**, 092507 (2009).
- <sup>31</sup> C. Kusko, R. S. Markiewicz, M. Lindroos, and A. Bansil, *Phys. Rev. B* **66**, 140513(R) (2002).
- <sup>32</sup> Tanmoy Das, R.S. Markiewicz, and A. Bansil, *Phys. Rev. Lett.* **98**, 197004 (2007).
- <sup>33</sup> Tanmoy Das, R.S. Markiewicz, and A. Bansil, *Phys. Rev. B* **77**, 134516 (2008).
- <sup>34</sup> M. Jarrell, Th. Maier, M. H. Hettler and A. N. Tahvildarzadeh, *Europhys. Lett.* **56**, 563 (2001).
- <sup>35</sup> J. L. Tallon, and J. G. Storey, arXiv:0908.4430.
- <sup>36</sup> Jinho Lee, K. Fujita, K. McElroy, J. A. Slezak, M. Wang, Y. Aiura, H. Bando, M. Ishikado, T. Masui, J.-X. Zhu, A.

- V. Balatsky, H. Eisaki, S. Uchida and J. C. Davis, *Nature* **442**, 546 (2006).
- <sup>37</sup> A. Bussmann-Holder, H. Keller, A. R. Bishop, A. Simon, K. A. Mueller, arXiv:0809.2881.
- <sup>38</sup> A. Macridin, and M. Jarrell, *Phys. Rev. B* **79**, 104517 (2009).
- <sup>39</sup> R.S. Markiewicz, J. Lorenzana, G. Seibold, and A. Bansil, *Phys. Rev. B* **81**, 014509 (2010); R.S. Markiewicz, J. Lorenzana, and G. Seibold, *Phys. Rev. B* **81**, 014510 (2010).
- <sup>40</sup> Tanmoy Das, R.S. Markiewicz, and A. Bansil, *Phys. Rev. B* **74**, 020506 (2006); *J. Phys. Chem. Solids* **69** 2963 (2008).
- <sup>41</sup> T. Yoshida, X J Zhou, D H Lu, Seiki Komiyama, Yoichi Ando, H Eisaki, T Kakeshita, S Uchida, Z Hussain, Z-X Shen and A Fujimori, *J. Phys.: Cond. Matt.* **19**, 125209 (2007).
- <sup>42</sup> G. Vignale and M. R. Hedayati, *Phys. Rev. B.*, **42**, 786 (1990).
- <sup>43</sup> R. S. Markiewicz, Tanmoy Das, Susmita Basak, A. Bansil, International Workshop on Strong Correlations and Angle-Resolved Photoemission Spectroscopy, 2009, Zurich, Switzerland, to be published.
- <sup>44</sup> J. R. Schrieffer, X. G. Wen, and S. C. Zhang, *Phys. Rev. B.* **39**, 11663 (1989).
- <sup>45</sup> R.S. Markiewicz, S. Sahrakorpi, M. Lindroos, Hsin Lin, and A. Bansil, *Phys. Rev. B* **72**, 054519 (2005).
- <sup>46</sup> R. S. Markiewicz, and A. Bansil, *Phys. Rev. B* **78**, 134513 (2008).
- <sup>47</sup> L. A. Bansil, U. Welp, Y. Fang and K. G. Bailey, *J. Phys. Chem. Solids* **52**, 1541 (1991).